nature biotechnology

Directed evolution of a magnetic resonance imaging contrast agent for noninvasive imaging of dopamine

Mikhail G Shapiro[1,5], Gil G Westmeyer[2,5], Philip A Romero[3], Jerzy O Szablowski[1], Benedict Küster[2], Ameer Shah[1], Christopher R Otey[3], Robert Langer[1], Frances H Arnold[3] & Alan Jasanoff[1,2,4]

The development of molecular probes that allow *in vivo* imaging of neural signaling processes with high temporal and spatial resolution remains challenging. Here we applied directed evolution techniques to create magnetic resonance imaging (MRI) contrast agents sensitive to the neurotransmitter dopamine. The sensors were derived from the heme domain of the bacterial cytochrome P450-BM3 (BM3h). Ligand binding to a site near BM3h's paramagnetic heme iron led to a drop in MRI signal enhancement and a shift in optical absorbance. Using an absorbance-based screen, we evolved the specificity of BM3h away from its natural ligand and toward dopamine, producing sensors with dissociation constants for dopamine of 3.3–8.9 μM. These molecules were used to image depolarization-triggered neurotransmitter release from PC12 cells and in the brains of live animals. Our results demonstrate the feasibility of molecular-level functional MRI using neural activity–dependent sensors, and our protein engineering approach can be generalized to create probes for other targets.

MRI is a uniquely valuable tool for studying the brain because MRI scans are noninvasive and can provide information at relatively high spatial resolution (< 100 μm) and temporal resolution (~1 s) from living specimens. Functional imaging (fMRI) of brain activity is possible with MRI methods sensitive to cerebral hemodynamics[1]. The most common fMRI technique, blood oxygen level–dependent (BOLD) fMRI, is based on oxygenation of hemoglobin, an endogenous oxygen-sensitive MRI contrast agent present in the blood[2]. Although BOLD fMRI has had a tremendous impact in neuroscience, the method provides only a slow and indirect readout of neural activity, owing to the complexity of neurovascular coupling[3]. Considerably more precise measurements of brain function would be possible with MRI sensors that were directly and rapidly responsive to neurochemicals involved in the brain's information processing[4].

The challenging process of developing sensors for next-generation neuroimaging could be greatly accelerated using advanced molecular engineering techniques. Directed evolution is a molecular engineering method that employs successive rounds of mutagenesis and selection to generate proteins with novel functionality, starting from a molecule with some of the desired properties of the end product[5]. This technique could be applied to evolve MRI sensors from proteins that are magnetically active (for example, paramagnetic) and have tunable ligand-binding or catalytic properties.

The flavocytochrome P450-BM3 (BM3), a fatty acid hydroxylase from *Bacillus megaterium*, contains a paramagnetic iron atom embedded in a solvent-accessible substrate-binding pocket, suggesting that it could produce ligand-dependent MRI signal changes. BM3's binding specificity is also highly tunable, as demonstrated by previous efforts to identify novel enzymatic activities through directed evolution of this protein[6–9]. If BM3 variants could be engineered to act as MRI sensors, they would be genetically encodable, an added advantage over synthetic molecular imaging agents.

We sought to apply directed evolution of BM3 to develop MRI sensors for a key signaling molecule in the brain, the neurotransmitter dopamine. To our knowledge, no MRI contrast agent for sensing dopamine (or any other neurotransmitter) currently exists, but there is considerable interest in measuring dopamine-related activity by MRI[10]. Dopamine is of particular significance because of its roles in learning, reward and motor coordination[11], and because the dysfunction of dopaminergic systems underlies addiction[12] and several neurodegenerative diseases[13]. Existing techniques for measuring dopamine *in vivo* are either invasive point-measurement methods[14–16] or positron emission tomography procedures[17] with low spatial and temporal resolution. MRI could be used successfully for dopamine measurement if combined with an imaging agent capable of responding quickly, reversibly and specifically to extracellular dopamine fluctuations from <1 μM to tens of micromolar[18,19]. To be comparable with established functional brain imaging techniques, interaction of dopamine with the probe should also produce image signal changes on the order of 1% or more *in vivo*[20]. Here we show that directed evolution of BM3 is capable of producing dopamine sensors that largely meet these specifications.

RESULTS

P450 BM3 reports ligand binding in MRI

To evolve dopamine probes for MRI, we focused on the heme domain of BM3 (BM3h), a 53-kDa moiety that is catalytically inactive in the absence of the full protein's reductase domain[21]. BM3h contains a

[1]Department of Biological Engineering and [2]Department of Brain & Cognitive Sciences, Massachusetts Institute of Technology, Cambridge, Massachusetts, USA. [3]Division of Chemistry & Chemical Engineering, California Institute of Technology, Pasadena, California, USA. [4]Department of Nuclear Science & Engineering, Massachusetts Institute of Technology, Cambridge, Massachusetts, USA. [5]These authors contributed equally to this work. Correspondence should be addressed to A.J. (jasanoff@mit.edu).

Received 25 June 2009; accepted 27 January 2010; published online 28 February 2010; doi:10.1038/nbt.1609

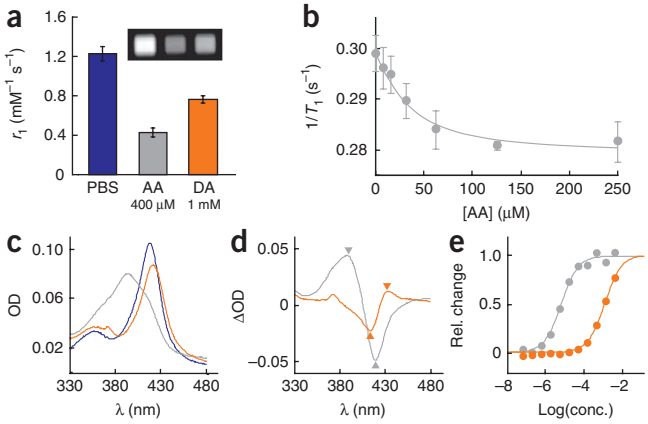

Figure 1 Ligand binding to the BM3 heme domain changes MRI contrast and optical absorption in a concentration-dependent manner. (**a**) T_1 relaxivity (r_1) of BM3h in PBS solution and in the presence of 400 μM arachidonic acid (AA) or 1 mM dopamine (DA); inset shows T_1-weighted spin echo MRI image intensity (TE/TR = 10/477 ms) of microtiter plate wells containing 240 μM BM3h in PBS alone (left) or in the presence of 400 μM arachidonic acid (middle) or 1 mM dopamine (right). (**b**) T_1 relaxation rates ($1/T_1$) measured from solutions of 28.5 μM BM3h incubated with 0–250 μM arachidonic acid. (**c**) Optical absorbance spectra of 1 μM BM3h measured alone (blue) and after addition of 400 μM arachidonic acid (gray) or 1 mM dopamine (orange). OD, optical density. (**d**) Difference spectra showing the change in BM3h absorbance as a function of wavelength upon addition of 400 μM arachidonic acid (gray) or 1 mM dopamine (orange). (**e**) Normalized titration curves showing binding of BM3h to arachidonic acid (gray) or dopamine (orange). We computed the optical signals used for titration analysis by subtracting the minimum from the maximum of difference spectra (arrowheads in **d**) under each set of conditions. Error bars in **a**, **b** and **e** reflect s.e.m. of three independent measurements (errors in **e** were smaller than the symbols).

single iron(III) atom (mixed spin 1/2 and 5/2)[22] bound to a hemin prosthetic group and axially coordinated by residue Cys400 on the protein. In the absence of substrates, the remaining coordination site is filled by a water molecule[23]. Interaction of the heme iron with exchanging water molecules at this axial site promotes T_1 relaxation in aqueous solutions[24] and is therefore predicted to modulate MRI contrast. To determine the extent of this effect, we used a spin echo pulse sequence in a 4.7-T MRI scanner to measure the proton relaxation rate as a function of protein concentration in PBS; the slope of this relationship (T_1 relaxivity, or r_1) provides a standard measure of the strength of a contrast agent. For BM3h in the absence of ligands, an r_1 value of 1.23 ± 0.07 mM^{-1} s^{-1} was obtained. Addition of a saturating quantity of the natural BM3 substrate, arachidonic acid (400 μM concentration), resulted in an r_1 of 0.42 ± 0.05 mM^{-1} s^{-1} (**Fig. 1a**). This ligand-induced decrease in relaxivity, probably arising from the displacement of water molecules at the BM3h heme, enabled quantitative sensing of arachidonic acid using MRI (**Fig. 1b**) and suggested that BM3h could serve as a platform for molecular sensor engineering.

We next tested whether dopamine or related compounds could serve as unnatural ligands to BM3h when applied at high enough concentrations. As measured by MRI, addition of 1 mM dopamine to BM3h in fact induced a drop in r_1 to 0.76 ± 0.03 mM^{-1} s^{-1} (**Fig. 1a**). Binding of arachidonic acid is known to induce a change (blue shift) in BM3h's optical absorbance spectrum because of perturbation of the electronic environment of the heme chromophore[25]. To determine whether the relaxation change induced by dopamine also reflects interaction with the BM3h heme, we measured optical spectra of the protein in the presence and absence of 1 mM dopamine. The interaction produced a small but clearly discernable red shift of λ_{max}, from 419 to 422 nm (**Fig. 1c**), indicative of ligand coordination to the heme iron[25]. This suggests that dopamine (at 1 mM) directly replaces water as an axial metal ligand in the BM3h substrate-binding pocket and that directed evolution of BM3h binding specificity could therefore improve the protein's relative affinity for dopamine. In addition to providing mechanistic insight, the correspondence between optical and MRI measurements of ligand binding to BM3h implied that either modality could be used to obtain quantitative binding parameters. We monitored the difference between absorption at two wavelengths as a function of ligand concentration to determine binding isotherms for arachidonic acid and dopamine (**Fig. 1d**,**e**). For BM3h, the apparent K_d for arachidonic acid was 6.8 ± 0.5 μM; the K_d for dopamine was 990 ± 110 μM. Goals for the production of BM3h-based MRI sensors thus included decreasing the affinity for arachidonic acid, increasing the dopamine affinity by at least two orders of magnitude and maintaining or enhancing the relaxivity changes observed upon ligand binding.

Directed evolution of dopamine-responsive BM3h variants

To create an MRI sensor for dopamine using directed evolution, we developed a customized screening methodology (**Fig. 2a**). Results shown in **Figure 1** suggested that either MRI-based or optical assays could be used to distinguish BM3h mutants with differing ligand affinities. We chose an absorbance assay for our screen because lower protein concentrations (~1 μM) could be used in this format. Input to each round of screening consisted of a library of BM3h mutants, each with an average of one to two amino acid substitutions, generated by error-prone PCR from the wild-type (WT) gene or a previously selected mutant. We transformed DNA libraries into *Escherichia coli*. We grew and induced approximately 900 randomly selected clones in microtiter plate format, then prepared cleared lysates for optical titration with dopamine and arachidonic acid in a plate reader. Titration data were analyzed to determine K_d values for both ligands. An average of 79% of assayed mutants had sufficient protein levels (absorbance signal > 30% of parent) and clean enough titration curves ($r^2 > 0.8$) for K_d estimation. Mutant affinities appeared to be distributed randomly about the dissociation constant measured for the corresponding parent protein, but we were able to identify individual clones with desired affinity changes in each round (**Fig. 2b**). From each screen, we chose eight to ten mutants on the basis of their estimated K_ds, purified them in bulk, re-titrated them to obtain more accurate estimates of their dopamine and arachidonic acid affinities, and examined them with MRI to ensure that robust ligand-induced changes in r_1 could be detected. On the basis of these assays, we chose as a parent for the next round of evolution the mutant showing the best combination of relaxivity changes, improved dopamine affinity and decreased affinity for arachidonic acid.

After carrying out the screening strategy over multiple rounds, we found a steady trend in the distribution of K_d values toward greater affinity for dopamine and less affinity for arachidonic acid (**Fig. 2b–d**). Little change in binding cooperativity was observed, and changes in partial saturation generally occurred over 100-fold ranges of dopamine concentrations. Five rounds of evolution yielded a BM3h variant with eight mutations (**Fig. 2e**), four near the ligand-binding pocket and four at distal surfaces of the protein. One residue (Ile263) was first mutated to threonine (third round), then to alanine (fourth round). The clones selected from rounds 1, 3 and 5 had two new mutations each. We did not determine the individual contributions of

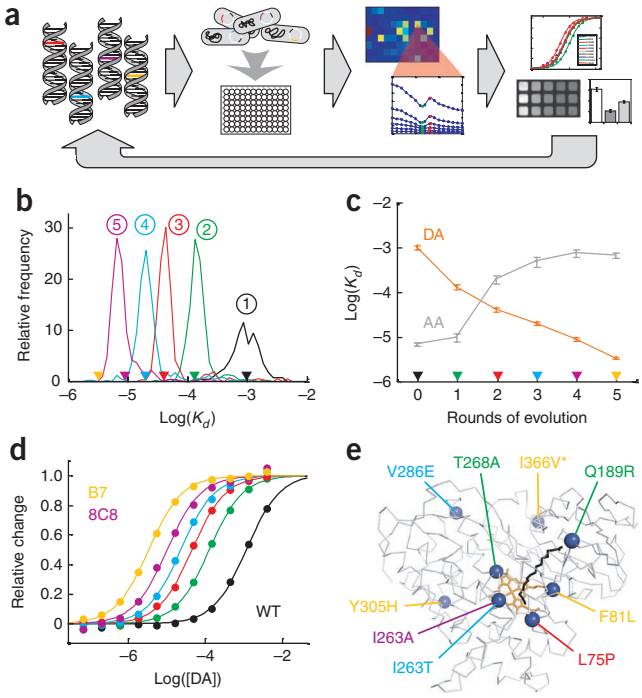

Figure 2 Screen-based isolation of BM3h mutants with enhanced dopamine affinity. (**a**) Schematic of the directed evolution approach, including (left to right) generation of a mutant DNA library, transformation into *E. coli* and growth in multiwell plate format, spectroscopic analysis of each mutant's ligand binding affinities, and detailed MRI and optical characterization of selected mutant proteins. (**b**) Histograms of mutant dopamine dissociation constants determined during each round of directed evolution, comparing each mutant protein's relative dopamine affinity (measured in plate format) to the K_d of the parent protein (measured in bulk). K_d distributions for screening rounds 1 (black), 2 (green), 3 (red), 4 (cyan) and 5 (purple) are labeled with numbers in circles. Color-coded arrowheads indicate the measured K_ds of parent proteins used to create the library of mutants at each round; yellow arrowhead indicates the K_d of the mutant protein selected after round 5. (**c**) Dissociation constants for dopamine (DA; orange) and arachidonic acid (AA; gray) for WT BM3h and mutant BM3h variants isolated at each round of screening; progressive increases in dopamine affinity and attenuation of arachidonic acid affinity are evident. Colored arrowheads indicate correspondence with data in **b**. Error bars denote s.e.m. of three independent measurements. (**d**) Titration analysis of dopamine binding to WT BM3h and to proteins selected after each round of directed evolution (colored as in **b**). Mutant proteins identified by rounds 4 (8C8) and 5 (B7) were considered to be end products of the screening procedure. (**e**) X-ray crystal structure[34] of WT BM3h (gray; heme group shown in orange) bound to palmitoleic acid (black), indicating the locations of amino acid substitutions accumulated during directed evolution of enhanced dopamine binding affinity. Each mutation's location is marked with a blue sphere and a label color-coded according to the parent protein in which the substitution was first identified (see legend for **b**). The previously characterized I366V mutation (asterisk) was incorporated between screening rounds 4 and 5 to improve the thermostability of the engineered proteins.

these mutations to the observed changes in affinity. We introduced the mutation I366V by site-directed mutagenesis before the fifth round to enhance thermostability and tolerance of BM3h to further mutation[26,27]; it did not noticeably affect dopamine binding affinity.

The mutant proteins selected after the fourth and fifth rounds of evolution, denoted BM3h-8C8 and BM3h-B7, had optically determined dissociation constants of 8.9 ± 0.7 μM and 3.3 ± 0.1 μM, respectively, for dopamine, and 750 ± 140 μM and 660 ± 80 μM, respectively, for arachidonic acid. The T_1 relaxivity of BM3h-8C8 was 1.1 ± 0.1 mM^{-1} s^{-1} in the absence of ligand and 0.17 ± 0.03 mM^{-1} s^{-1} in the presence of 400 μM dopamine (**Fig. 3a**). For BM3h-B7, the corresponding r_1 values were 0.96 ± 0.13 mM^{-1} s^{-1} and 0.14 ± 0.04 mM^{-1} s^{-1}. Both sensor variants showed a dopamine concentration–dependent decrease in T_1-weighted MRI signal (up to 13% with 28.5 μM protein) that could be fitted by binding isotherms with estimated K_d values of 4.9 ± 2.7 μM for BM3h-8C8 and 2.7 ± 2.9 μM for BM3h-B7 (**Fig. 3b,c**). For both BM3h variants, the stability, reversibility and rate of dopamine binding were established using spectroscopic assays (**Supplementary Figs. 1** and **2**).

We investigated the reporting specificities of BM3h-8C8 and BM3h-B7 for dopamine by measuring MRI signal changes that resulted from incubation of 28.5 μM of each protein with 30 μM of either dopamine or one of eight other neuroactive molecules: norepinephrine (a neurotransmitter formed by catalytic hydroxylation of dopamine), 3,4-dihydroxy-L-phenylalanine (DOPA, the biosynthetic precursor to dopamine), serotonin, glutamate, glycine, γ-aminobutyric acid (GABA), acetylcholine and arachidonic acid (**Fig. 3d**). Of these potential ligands, only dopamine, norepinephrine and serotonin elicited

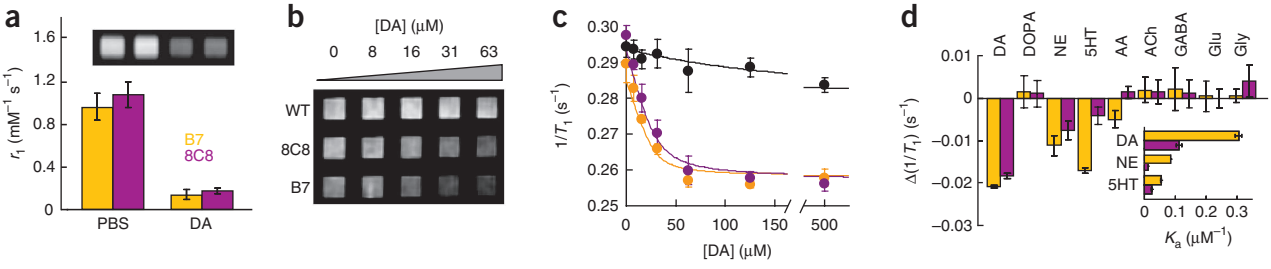

Figure 3 Selected sensor proteins produce strong and specific MRI signal changes in response to dopamine. (**a**) Relaxivity values measured from BM3h-B7 (yellow bars) and BM3h-8C8 (purple bars) in PBS alone or in the presence of 400 μM dopamine (DA). Inset, T_1-weighted MRI signal (TE/TR = 10/477 ms) obtained from 195 μM BM3h-B7 or BM3h-8C8, each incubated in microtiter plate wells with or without 400 μM dopamine (wells ordered left to right as in the bar graph). (**b**) MRI image showing signal amplitudes measured from wells containing 28.5 μM WT BM3h, BM3h-8C8 or BM3h-B7, each incubated with increasing dopamine concentrations (0–63 μM, left to right). The image was obtained using a T_1-weighted pulse sequence (TE/TR = 10/477 ms). (**c**) Relaxation rates ($1/T_1$ values) measured from solutions of 28.5 μM WT BM3h (black), BM3h-B7 (yellow) or BM3h-8C8 (purple), as a function of total dopamine concentration. Curves were fitted using a ligand-depleting bimolecular association model. (**d**) Changes in $1/T_1$ relative to ligand-free protein for 28.5 μM BM3h-B7 (yellow) or BM3h-8C8 (purple) incubated with 30 μM dopamine, serotonin (5HT), norepinephrine (NE), DOPA, arachidonic acid (AA), acetylcholine (ACh), GABA, glutamate or glycine. Inset, spectroscopically determined affinities ($K_a = 1/K_d$) of BM3h-B7 and BM3h-8C8 for dopamine, serotonin and norepinephrine. Error bars in panels **a**, **c** and **d** denote s.e.m. of three independent measurements.

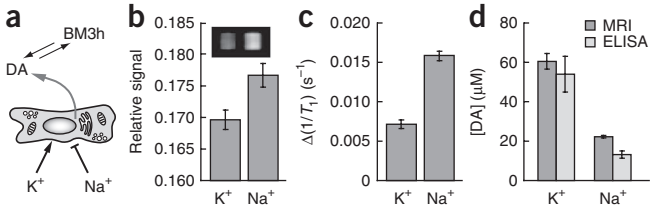

Figure 4 BM3h-based sensors measure dopamine release in cell culture. (**a**) PC12 cells depolarized by addition of 54 mM K^+ were stimulated to release dopamine (DA) into supernatants containing a BM3h-based sensor; cells did not release dopamine after addition of 54 mM Na^+. (**b**) T_1-weighted spin echo MRI signal amplitudes (TE/TR = 10/477 ms) measured from the supernatants of PC12 cells incubated with 32 μM BM3h-B7 in the presence of K^+ (stimulus) or Na^+ (control). Inset, MRI image of microtiter wells under corresponding conditions. (**c**) Relaxation rates measured from the samples in **b**, minus the relaxation rate of buffer not containing BM3h-based sensors. Given the approximate concentration of BM3h variants in these samples, the $\Delta(1/T_1)$ values presented here can be converted to apparent relaxivities of 0.23 and 0.50 mM^{-1} s^{-1} in K^+ and Na^+ incubation conditions, respectively. (**d**) Data from **c** were used to estimate the concentrations of dopamine present in samples treated with K^+ and Na^+ (dark bars). We independently measured the concentrations of dopamine under equivalent conditions using ELISA (light bars).

substantial changes in the T_1 relaxation rate ($1/T_1$). For BM3h-8C8, the $1/T_1$ reductions produced by norepinephrine and serotonin were 0.0076 ± 0.0023 s^{-1} and 0.0041 ± 0.0020 s^{-1}, respectively, compared to 0.0182 ± 0.0006 s^{-1} for dopamine; for BM3h-B7, norepinephrine and serotonin induced $1/T_1$ decreases of 0.0112 ± 0.0024 s^{-1} and 0.0171 ± 0.0005 s^{-1}, respectively, compared to 0.0208 ± 0.0002 s^{-1} for dopamine. We measured the affinities of BM3h-based dopamine sensors for these competitors spectroscopically (**Fig. 3d**, inset). For BM3h-8C8, measured K_ds were 44 ± 3 μM and 80 ± 8 μM for norepinephrine and serotonin, respectively, and for BM3h-B7 the K_d values were 18.6 ± 0.4 μM and 11.8 ± 0.1 μM, respectively. Although both BM3h-8C8 and BM3h-B7 show substantially higher affinity for dopamine than for norepinephrine (fivefold and sixfold, respectively) or for serotonin (ninefold and fourfold, respectively), the BM3h-8C8 variant is more specific for sensing dopamine at concentrations above 10 μM. In settings where dopamine is known to be the dominant neurotransmitter, BM3h-B7 may provide greater overall sensitivity.

The specificity data also provided a possible indication of the geometry of dopamine binding to the evolved BM3h proteins. Only monoamines showed affinity for BM3h-8C8 and BM3h-B7, whereas two catechols that lack primary amines, epinephrine and 3,4-dihydrophenylacetic acid, showed no measurable affinity (data not shown). Combined with the spectral evidence that dopamine directly coordinates the BM3h heme (**Fig. 1c**), the titration results therefore suggest that the dopamine amine may serve as an axial ligand to the BM3h heme in the sensor-analyte complexes we examined.

BM3h-based sensors detect dopamine released from PC12 cells

We asked whether BM3h mutants produced by directed evolution could sense dopamine release in a standard cellular model of dopaminergic function. We applied an established protocol[28] to test the ability of our sensors to measure dopamine discharge from PC12 cells stimulated with extracellular K^+ (**Fig. 4a**). Cells were cultured in serum-free medium supplemented with dopamine to promote packaging of the neurotransmitter into vesicles. After pelleting and washing, we resuspended cells in a physiological buffer containing 32 μM BM3h-B7 and either 5.6 or 59.6 mM K^+ (cells in the low-K^+ condition were osmotically balanced with Na^+). T_1-weighted MRI images (spin echo TE/TR = 10/477 ms) obtained with BM3h-B7 showed a 4.0 ± 0.5% reduction in signal intensity in the supernatant of K^+-stimulated cells, compared with cells for which isotonic Na^+ was used as control (**Fig. 4b**). This corresponded to a 54 ± 4% decrease in sensor r_1 (**Fig. 4c**). Given the dopamine dissociation constant of BM3h-B7 and its relaxivities under ligand-free and dopamine-saturated conditions, and assuming negligible dilution of the sensor after mixing with cells, we estimated supernatant dopamine concentrations of 60.3 ± 7.9 μM for stimulated cells and 22.2 ± 1.1 μM for controls. These estimates were in reasonable agreement with an independent quantification of dopamine release measured using an enzyme-linked immunosorbent assay (ELISA), which yielded concentrations of 54 ± 9 μM and 13 ± 2 μM for stimulated and control cells, respectively (**Fig. 4d**). We were also able to use BM3h-8C8 to image dopamine release from PC12 cells. Under experimental conditions similar to above, BM3h-8C8 had a 37 ± 2% reduction in r_1 in the supernatant of K^+-stimulated cells relative to Na^+ controls (**Supplementary Fig. 3**).

Dopamine detection in the brain of living rats

As an initial test of the ability of BM3h-based sensors to measure dopamine concentrations in intact animals, we injected BM3h-8C8 in the presence or absence of exogenous dopamine into the brains of anesthetized rats. We chose this simple experimental protocol for validation of the sensor because it guaranteed the presence of reproducible and unambiguous micromolar-level dopamine concentrations, suitable for evoking robust responses from our sensors *in vivo*. We obtained T_1-weighted MRI scans (fast spin echo TE/TR 14/277 ms, 8.9 s per image) continuously during 0.5-μl-min^{-1} paired infusions of 500 μM BM3h-8C8 with and without 500 μM dopamine, via cannulae implanted stereotaxically into the left and right striatum. Dopamine-dependent contrast changes were apparent in images obtained during and after the injection period (**Fig. 5a**). We quantified MRI changes across multiple trials in striatal regions of interest (ROIs) that were reliably (though inhomogeneously) filled by convective spread of the contrast agent from the cannula tips (~1.5 mm radius). Consistent with results obtained *in vitro*, addition of dopamine dampened the observed MRI intensity enhancement by approximately 50% (**Fig. 5b**); the effect was significant (*t*-test, $P = 0.003$, $n = 7$). We performed the same paired infusion procedure with WT BM3h, which has very low affinity for dopamine (K_d ~1 mM). As expected, the time course of the MRI signal during and after the WT BM3h injection period (**Fig. 5c**) was not significantly affected by the presence or absence of dopamine (*t*-test, $P = 0.8$, $n = 5$), indicating that the dopamine-dependent signal differences shown in **Figure 5b** require the presence of a micromolar-affinity dopamine sensor and cannot be explained by physiological or biochemical effects of dopamine itself. Moreover, infusion of 500 μM dopamine alone into the brain produced no noticeable signal changes in an equivalent experiment (data not shown). Histological analysis showed minimal evidence of toxicity due to these procedures (**Supplementary Fig. 4**). Using relaxivity values measured for BM3h-8C8 *in vitro*, we estimated maximal concentrations of 89 ± 19 μM BM3h-8C8 and 75 ± 28 μM dopamine from the data of **Figure 5b**, averaged across the striatal ROIs. The ability to quantify BM3h-8C8 concentration on the basis of its T_1 enhancement in the absence of elevated dopamine represents an advantage of this sensor's 'turn-off' mechanism.

To test whether BM3h-8C8 could detect release of endogenous neurotransmitters in the rat brain, we acquired MRI data during co-infusion of the dopamine sensor with elevated concentrations of K^+, a depolarizing chemical stimulus shown previously to release large amounts of

dopamine into the striatum[29,30]. We chose K^+ over pharmacological stimuli to obviate potential solubility- or viscosity-related artifacts in the experimental paradigm. K^+ itself had no effect on r_1 of the BM3h variants (data not shown). In the stimulation experiments, three 5-min blocks of high-K^+ (153 mM) infusion alternated with 10-min 'rest' periods during which we administered a low-K^+ solution (3 mM, osmotically balanced with Na^+). Both high- and low-K^+ solutions were delivered at a rate of 0.2 µl min^{-1} and also contained 500 µM BM3h-8C8, ensuring that a relatively constant concentration of dopamine sensor was present throughout the procedure. We acquired T_1-weighted MRI scans continuously as for the exogenous dopamine infusion experiments. To control for effects unrelated to neurotransmitter sensing by the contrast agent (potentially including K^+-induced edema or hemodynamic responses incompletely suppressed by the T_1-weighted spin echo pulse sequence), we paired each striatal injection of BM3h-8C8 with an injection of WT BM3h into the opposite hemisphere, following the same blocked K^+ stimulation paradigm for both injections. As in conventional 'block design' fMRI, we performed a *t*-test analysis to evaluate the correspondence of each voxel's intensity time course with the alternating periods of low and high K^+. We determined an appropriate temporal shift for the stimulus-related analysis windows with respect to infusion buffer switches by observing the time courses of similarly switched mock infusions into 0.6% agarose phantoms[31] and by comparing these with statistical results as a function of offset (**Supplementary Fig. 5** and Online Methods). As additional controls for MRI effects unrelated to dopamine sensing, we examined MRI signal change in response to K^+ stimulation and again in response to dopamine infusion, both in the absence of contrast agents (data not shown). We also continuously monitored blood oxygen levels and heart rate. In no case were stimulus-associated changes observed.

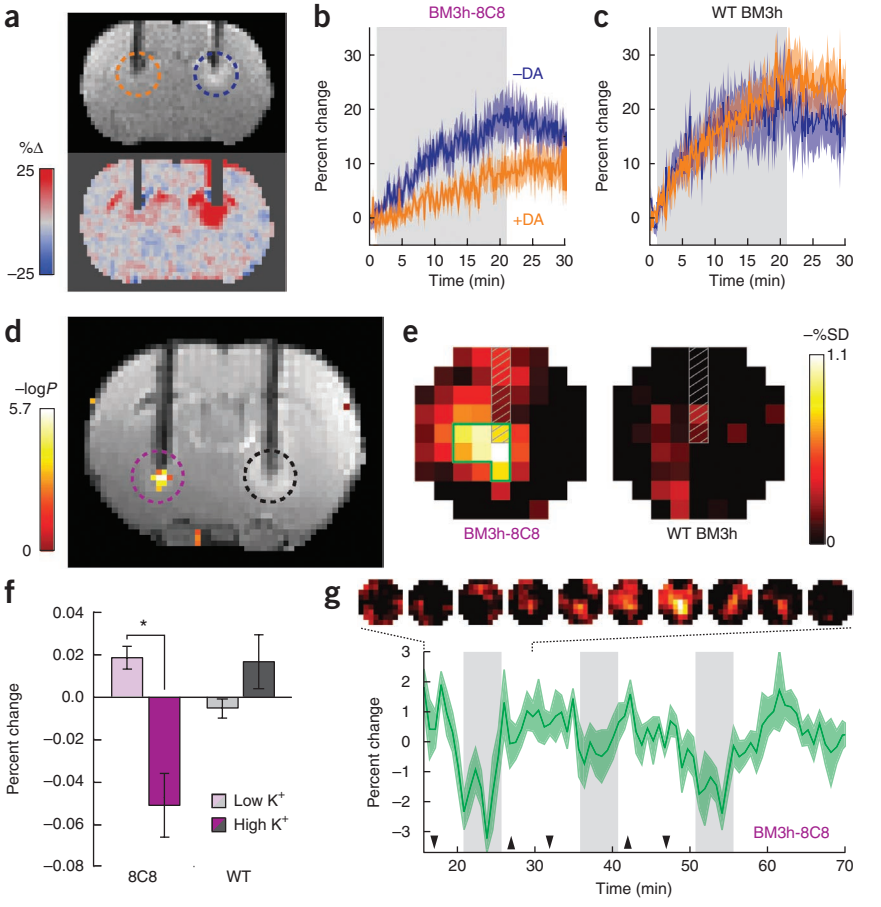

Figure 5 BM3h-8C8 reports dopamine in injected rat brains. (**a**) Top, coronal MRI image (0.7 mm anterior to bregma, averaged over the injection period) from a single rat injected with 500 µM BM3h-8C8 in the presence (orange dashed circle) or absence (blue dashed circle) of equimolar dopamine; the image contrast was linearly adjusted for display. MRI hyperintensity is noticeable near the tip of the dopamine-free cannula. The circles indicate approximate ROIs (~1.5 mm around cannula tips) over which image intensity was averaged for quantitative analyses. Bottom, map of percent signal change (%Δ) for the same animal, computed by comparing pre- and post-injection MRI signal. Areas corresponding to both high- and low-dopamine co-injections (+DA and –DA) are delineated by apparent signal changes, but the strong difference between the two conditions is clear. (**b**) Time courses of relative signal change observed during injection of BM3h-8C8 –DA (blue) or +DA (orange), averaged over multiple animals ($n = 7$) in ROIs denoted in **a**. Gray shading denotes the 20-min injection period. (**c**) Corresponding time courses of a control injection in which WT BM3h was introduced instead of the dopamine sensor ($n = 5$). (**d**) Statistical parametric map of *t*-test significance values (color scale) for correlation of MRI intensity with low- and high-K^+ conditions in an individual rat, overlaid on a corresponding T_1-weighted coronal slice (grayscale) showing injection cannulae used for BM3h-8C8 infusion (left, purple dashed circle) and WT BM3h control infusion (right, black dashed circle). (**e**) Maps of percent signal difference (SD) between high- and low-K^+ conditions observed in 2.7-mm-diameter ROIs centered around BM3h-8C8 sensor (left) and WT BM3h control (right) injection sites, after spatial coregistration and averaging across multiple animals ($n = 6$); ROIs correspond approximately to the color-coded circles in **d**. Voxels outlined in green are those that showed the most significant correlation with the K^+ stimulus regressor in the group analysis (Student's *t*-test, $P < 0.01$); these generally showed ~1% mean signal change. Gray cross-hatching indicates approximate locations of the infusion cannulae. (**f**) Mean MRI signal change from baseline observed during high-K^+ (dark bars) and low-K^+ (light bars) periods in ROIs centered around infusion sites for BM3h-8C8 (purple) and WT BM3h (gray) proteins. ROIs were cylinders 2.7 mm in diameter and extending over three 1-mm-thick slices registered around the infusion sites; signal was averaged in unbiased fashion over all voxels, regardless of correlation with the stimulus. The signal difference in the presence of BM3h-8C8 was statistically significant ($P = 0.0008$, asterisk). (**g**) Graph shows the mean time course of MRI signal in voxels within the BM3h-8C8–infused ROI and identified as correlated ($P < 0.05$) with the stimulus, averaged over animals and binned over 1.5-min intervals (shaded area denotes s.e.m., $n = 6$; individual traces are shown in **Supplementary Fig. 6** online). Gray vertical bars denote periods associated with highest K^+ stimulation, accounting for delays due to convective spreading of K^+ from the cannulae tips and the dead time of the injection apparatus. Arrowheads indicate the timing of pump switches associated with transitions from low to high (up) and from high to low (down) K^+ infusion conditions. Panels above the graph depict 'snapshots' of signal change spaced throughout the first K^+ stimulation cycle, as indicated by the dotted lines. The ROI corresponds to the left side of **e**, and the color scale denotes 0% (black) to 3% (yellow) signal change from baseline at each voxel and time point.

Figure 5d shows the distribution of voxels with significant (*t*-test, $P < 0.01$) MRI signal decreases in response to K^+ stimulation in a single rat. We performed a group analysis by combining data from all subjects ($n = 6$) over geometrically defined ROIs centered around the injection cannula tips in each animal. In three slices spanning the infusion site, seven voxels within 0.75 mm of the BM3h-8C8 injection cannula, but only one voxel near the WT cannula, showed strong correlation ($P < 0.01$) with the stimulus. We mapped mean signal decreases over 2.7-mm-diameter ROIs corresponding to the BM3h-8C8 and WT BM3h injection sites in the group analysis (**Fig. 5e**). Again, dopamine sensor–dependent responses were apparent. The signal difference between low- and high-K^+ periods averaged across the entire BM3h-8C8 ROI (all voxels within a 2.7-mm-diameter by 3-mm-long cylinder, regardless of modulation by K^+) was 0.07%, whereas the signal difference averaged across the control ROI was −0.02% (**Fig. 5f**). The high- versus low-K^+ signal difference observed near the BM3h-8C8 infusion site was significant (*t*-test, $P = 0.0008$) and consistent with the expected suppression of MRI signal by dopamine release under high-K^+ conditions.

The mean time course of all stimulus-correlated voxels ($P < 0.05$) showing K^+-induced MRI signal changes near the BM3h-8C8 injection site, averaged over animals, is shown in **Figure 5g**. Discernable signal decreases of up to 3% were produced during each K^+ stimulation block. The first K^+ block evoked the largest response (presumably because of partial dopamine depletion over subsequent blocks[32]) and elicited a clear spatiotemporal pattern of mean MRI signal change from baseline over the course of the stimulation period (**Fig. 5g**, top panels).

DISCUSSION

These results demonstrate the feasibility of developing molecular-level fMRI sensors and serve as a proof of principle that BM3h-based probes can be used to monitor dopamine signaling processes *in vivo*. With the experimental conditions and estimated sensor concentrations (34 ± 4 μM) used for our K^+ stimulation experiments, MRI signal changes of ~3% would be evoked by the rewarding brain stimuli reported in previous studies to release large amounts of dopamine[18,19]. This amplitude is reasonably large by functional imaging standards, and it could be used in the near term to map phasic dopamine release at high resolution across the striatum, or more generally to study mesolimbic dopamine dynamics in animal models of reward processing and neurological conditions that can be probed with strong stimuli.

Sensitivity gains will be possible using repeated stimulation and statistical analysis techniques, as in conventional fMRI, and by optimizing the imaging approach itself. For instance, higher-field scanners and faster alternatives to the T_1-weighted spin echo pulse sequences we used here may offer improved signal-to-noise ratios. Directed evolution or rational modification of BM3h variants for substantially higher relaxivity is possible as well (unpublished data). Sensors with higher relaxivity will produce larger MRI signal changes, and could have the added benefit of reducing the potential for dopamine buffering, because they may be used at lower concentrations *in vivo*: with 35 μM sensor and 35 μM total dopamine present, for example, ~60% of the dopamine would be bound to the sensor, but with 15 μM sensor present, only ~30% dopamine would be sequestered. Protein engineering techniques could also be used to improve the dopamine affinity and specificity of the first-generation sensors described here.

Our method for producing dopamine sensors represents a general paradigm for the development of molecular probes for MRI. Sensors may be evolved for targets inside or outside the brain; the diversity of potential targets is exemplified by the contrast between WT BM3h, which produces MRI signal changes in response to long-chain fatty acids, and BM3h-8C8 and BM3h-B7, which respond to a catecholamine. Contrast agents engineered to detect dopamine and other signaling molecules in the brain will permit functional neuroimaging based on direct detection of neuronal events rather than hemodynamic changes. Exogenous delivery of macromolecules such as BM3h to large regions of animal brains should be possible using a variety of techniques[33]. Because BM3h is a protein, it might also be possible to deliver variants via expression from transfected cells *in vivo* or in transgenic subjects. Preliminary evidence that BM3h can be expressed to 1% protein content in mammalian cells supports the feasibility of this approach (**Supplementary Results**). Because of their small size, BM3h-based dopamine sensors might sample synaptic dopamine better than voltammetry or microdialysis probes, and with appropriate targeting could potentially become synapse specific. Dopamine sensor-dependent MRI would offer a combination of spatial coverage and precision inaccessible to other methods and uniquely suited to studies of dopaminergic function in systems neuroscience research.

METHODS

Methods and any associated references are available in the online version of the paper at http://www.nature.com/naturebiotechnology/.

Note: Supplementary information is available on the Nature Biotechnology website.

ACKNOWLEDGMENTS

We thank V. Lelyveld for helpful discussions and assistance with *in vitro* measurements, N. Shah for help with MRI procedures and W. Schulze for help with automated analysis methods. We are grateful to C. Jennings and D. Cory for comments and suggestions about the manuscript, and to D. Vaughan for consultation regarding histology. We thank P. Caravan and again D. Cory for access to low-field relaxometers. M.G.S. thanks the Fannie and John Hertz Foundation and the Paul and Daisy Soros Fellowship for generous support. This work was funded by a Dana Foundation Brain & Immuno-Imaging grant, a Raymond & Beverley Sackler Fellowship and US National Institutes of Health (NIH) grants R01-DA28299 and DP2-OD2441 (New Innovator Award) to A.J., NIH grant R01-GM068664 and a grant from the Caltech Jacobs Institute for Molecular Medicine to F.H.A. and NIH grant R01-DE013023 to R.L.

AUTHOR CONTRIBUTIONS

M.G.S. conceived and performed the directed evolution and *in vitro* assessment of dopamine sensors; G.G.W. designed and conducted the *in vivo* experiments; P.A.R. performed directed evolution screening for BM3h variants; J.O.S. assisted with screening and *in vitro* experiments; B.K. assisted with data analysis for *in vivo* experiments; A.S. assisted with *in vivo* experiments; C.R.O. worked with M.G.S. to establish BM3h screening methods; R.L. provided consultation and essential materials; F.H.A. supervised the directed evolution work; A.J. established research direction, supervised the project overall and co-wrote the paper with M.G.S. and G.G.W.

COMPETING INTERESTS STATEMENT

The authors declare no competing financial interests.

Published online at http://www.nature.com/naturebiotechnology/.
Reprints and permissions information is available online at http://npg.nature.com/reprintsandpermissions/.

1. Buxton, R.B. *Introduction to Functional Magnetic Resonance Imaging: Principles and Techniques* (Cambridge University Press, New York, 2001).
2. Ogawa, S., Lee, T.M., Kay, A.R. & Tank, D.W. Brain magnetic resonance imaging with contrast dependent on blood oxygenation. *Proc. Natl. Acad. Sci. USA* **87**, 9868–9872 (1990).
3. Logothetis, N.K. What we can do and what we cannot do with fMRI. *Nature* **453**, 869–878 (2008).
4. Jasanoff, A. MRI contrast agents for functional molecular imaging of brain activity. *Curr. Opin. Neurobiol.* **17**, 593–600 (2007).
5. Bloom, J.D. *et al.* Evolving strategies for enzyme engineering. *Curr. Opin. Struct. Biol.* **15**, 447–452 (2005).
6. Li, Q.S., Schwaneberg, U., Fischer, P. & Schmid, R.D. Directed evolution of the fatty-acid hydroxylase P450 BM-3 into an indole-hydroxylating catalyst. *Chemistry (Easton)* **6**, 1531–1536 (2000).

7. Glieder, A., Farinas, E.T. & Arnold, F.H. Laboratory evolution of a soluble, self-sufficient, highly active alkane hydroxylase. *Nat. Biotechnol.* **20**, 1135–1139 (2002).
8. Meinhold, P., Peters, M.W., Chen, M.M., Takahashi, K. & Arnold, F.H. Direct conversion of ethane to ethanol by engineered cytochrome P450 BM3. *ChemBioChem* **6**, 1765–1768 (2005).
9. Otey, C.R., Bandara, G., Lalonde, J., Takahashi, K. & Arnold, F.H. Preparation of human metabolites of propranolol using laboratory-evolved bacterial cytochromes P450. *Biotechnol. Bioeng.* **93**, 494–499 (2006).
10. Knutson, B. & Gibbs, S.E. Linking nucleus accumbens dopamine and blood oxygenation. *Psychopharmacology (Berl.)* **191**, 813–822 (2007).
11. Schultz, W. Multiple dopamine functions at different time courses. *Annu. Rev. Neurosci.* **30**, 259–288 (2007).
12. Hyman, S.E., Malenka, R.C. & Nestler, E.J. Neural mechanisms of addiction: the role of reward-related learning and memory. *Annu. Rev. Neurosci.* **29**, 565–598 (2006).
13. Damier, P., Hirsch, E.C., Agid, Y. & Graybiel, A.M. The substantia nigra of the human brain. II. Patterns of loss of dopamine-containing neurons in Parkinson's disease. *Brain* **122**, 1437–1448 (1999).
14. Young, A.M., Joseph, M.H. & Gray, J.A. Increased dopamine release *in vivo* in nucleus accumbens and caudate nucleus of the rat during drinking: a microdialysis study. *Neuroscience* **48**, 871–876 (1992).
15. Garris, P.A. & Wightman, R.M. Different kinetics govern dopaminergic transmission in the amygdala, prefrontal cortex, and striatum: an *in vivo* voltammetric study. *J. Neurosci.* **14**, 442–450 (1994).
16. Gubernator, N.G. *et al.* Fluorescent false neurotransmitters visualize dopamine release from individual presynaptic terminals. *Science* **324**, 1441–1444 (2009).
17. Lindsey, K.P. & Gatley, S.J. Applications of clinical dopamine imaging. *Neuroimaging Clin. N. Am.* **16**, 553–573 (2006).
18. Ewing, A.G., Bigelow, J.C. & Wightman, R.M. Direct *in vivo* monitoring of dopamine released from two striatal compartments in the rat. *Science* **221**, 169–171 (1983).
19. Michael, A.C., Ikeda, M. & Justice, J.B. Jr. Mechanisms contributing to the recovery of striatal releasable dopamine following MFB stimulation. *Brain Res.* **421**, 325–335 (1987).
20. Duong, T.Q., Kim, D.S., Ugurbil, K. & Kim, S.G. Spatiotemporal dynamics of the BOLD fMRI signals: toward mapping submillimeter cortical columns using the early negative response. *Magn. Reson. Med.* **44**, 231–242 (2000).
21. Munro, A.W. *et al.* P450 BM3: the very model of a modern flavocytochrome. *Trends Biochem. Sci.* **27**, 250–257 (2002).
22. Macdonald, I.D., Munro, A.W. & Smith, W.E. Fatty acid-induced alteration of the porphyrin macrocycle of cytochrome P450 BM3. *Biophys. J.* **74**, 3241–3249 (1998).
23. Ravichandran, K.G., Boddupalli, S.S., Hasermann, C.A., Peterson, J.A. & Deisenhofer, J. Crystal structure of hemoprotein domain of P450BM-3, a prototype for microsomal P450's. *Science* **261**, 731–736 (1993).
24. Modi, S. *et al.* NMR studies of substrate binding to cytochrome P450 BM3: comparisons to cytochrome P450 cam. *Biochemistry* **34**, 8982–8988 (1995).
25. Lewis, D.F.V.. *Guide to Cytochrome P450 Structure and Function* (Taylor & Francis, New York, 2001).
26. Fasan, R., Chen, M.M., Crook, N.C. & Arnold, F.H. Engineered alkane-hydroxylating cytochrome P450(BM3) exhibiting nativelike catalytic properties. *Angew. Chem. Int. Edn Engl.* **46**, 8414–8418 (2007).
27. Bloom, J.D., Labthavikul, S.T., Otey, C.R. & Arnold, F.H. Protein stability promotes evolvability. *Proc. Natl. Acad. Sci. USA* **103**, 5869–5874 (2006).
28. Ohnuma, K., Hayashi, Y., Furue, M., Kaneko, K. & Asashima, M. Serum-free culture conditions for serial subculture of undifferentiated PC12 cells. *J. Neurosci. Methods* **151**, 250–261 (2006).
29. Ewing, A.G., Wightman, R.M. & Dayton, M.A. *In vivo* voltammetry with electrodes that discriminate between dopamine and ascorbate. *Brain Res.* **249**, 361–370 (1982).
30. Gerhardt, G.A., Rose, G.M. & Hoffer, B.J. Release of monoamines from striatum of rat and mouse evoked by local application of potassium: evaluation of a new *in vivo* electrochemical technique. *J. Neurochem.* **46**, 842–850 (1986).
31. Chen, Z.J. *et al.* A realistic brain tissue phantom for intraparenchymal infusion studies. *J. Neurosurg.* **101**, 314–322 (2004).
32. Michael, A.C., Ikeda, M. & Justice, J.B. Jr. Dynamics of the recovery of releasable dopamine following electrical stimulation of the medial forebrain bundle. *Neurosci. Lett.* **76**, 81–86 (1987).
33. Vykhodtseva, N., McDannold, N. & Hynynen, K. Progress and problems in the application of focused ultrasound for blood-brain barrier disruption. *Ultrasonics* **48**, 279–296 (2008).
34. Li, H. & Poulos, T.L. The structure of the cytochrome p450BM-3 haem domain complexed with the fatty acid substrate, palmitoleic acid. *Nat. Struct. Biol.* **4**, 140–146 (1997).

ONLINE METHODS

Animal care. We performed all experiments involving vertebrate animals with approval of the Massachusetts Institute of Technology Committee on Animal Care.

Library construction. We constructed BM3h mutant libraries in accordance with a previously published protocol[7]. The starting parent for evolution was the WT heme domain of BM3 with a C-terminal hexahistidine tag, housed in the pCWori vector[35]. We produced mutant libraries through error-prone PCR using the primers 5′-GAAACAGGATCCATCGATGCTTAGGAGGTCAT-3′ (forward) and 5′-GCTCATGTTTGACAGCTTATCATCG-3′ (reverse) and Taq polymerase (AmpliTaq, Applied Biosystems) with 25 μM $MnCl_2$, producing ~1–2 mutations per gene. Between the fourth and fifth rounds of evolution, we introduced the mutation I366V into BM3h-8C8 via overlap extension PCR to improve protein thermostability[27].

Protein expression and high-throughput screening. We inoculated mutant colonies into deep-well 96-well plates containing 0.4 ml Luria broth (LB) medium and grew them overnight. On each plate, we included the parent clone and up to three previous parents in triplicate. We then transferred 0.1 ml of each culture to new plates containing 1.2 ml fresh terrific broth (TB) medium per well, supplemented with 100 μg ml^{-1} ampicillin, 0.2 mM isopropyl β-D-1-thiogalactopyranoside (IPTG) and 0.5 mM δ-aminolevulinic acid (ALA). We stored remaining LB cultures with glycerol at −80 °C. After 20–30 h of protein expression at 30 °C, we pelleted cultures and lysed the pellets in 0.65 ml PBS containing 0.75 mg ml^{-1} hen egg lysozyme (Sigma-Aldrich) and 5 μg ml^{-1} DNase I (Sigma-Aldrich). We recorded absorbance spectra of 200 μl of cleared lysate from each well in a multiwell plate reader (Spectramax Plus, Molecular Devices) before and after addition of successively more concentrated dopamine or arachidonic acid. We analyzed the resulting absorbance spectra in Matlab (Mathworks) using a custom routine that calculated the absorbance difference spectra for each acquisition relative to ligand-free lysate, computed the difference between maximum and minimum of each difference spectrum, plotted each value as a function of ligand concentration and, for each well, fitted a non-ligand-depleting bimolecular association function to estimate the corresponding K_d. We subsequently compared mutant K_d values to those of the parents within each plate and chose eight to ten mutants showing the greatest decrease in K_d for dopamine and/or the greatest increase in K_d for arachidonic acid for bulk expression and analysis.

Bulk expression and titrations. To produce selected proteins in bulk, we began by inoculating frozen LB cultures of candidate mutants into 30 ml TB medium containing 100 μg ml^{-1} ampicillin. We induced the cultures at log phase with 0.6 mM IPTG, supplemented them with 0.5 mM ALA and 50 μg ml^{-1} thiamine and shook them for an additional 20–25 h to express protein. We then lysed pelleted cells with BugBuster and Lysonase (EMD Chemicals) and purified BM3h mutants over Ni-NTA agarose (Qiagen). We exchanged buffer to PBS over PD-10 desalting columns (GE Healthcare), and measured protein concentration using a carbon monoxide binding assay[36]. To characterize ligand affinities of the purified variants, we titrated protein samples with dopamine, arachidonic acid, serotonin, norepinephrine, pyrocatechol, 3,4-dihydroxy-L-phenylalanine (DOPA), 3,4-dihydroxyphenylacetic acid (DOPAC), homovanillic acid (HVA), 3-methoxytyramine (3MT), acetylcholine, glutamate, glycine, GABA and epinephrine (all from Sigma Aldrich) and analyzed the results using Matlab as described above. We performed all measurements at room temperature (~21 °C). 3MT had a K_d of 73 ± 13 μM for BM3h-B7 and 183 ± 28 μM for BM3h-8C8. HVA and pyrocatechol showed no measurable affinity.

***In vitro* magnetic resonance imaging.** To assess magnetic relaxation behavior of the proteins, we arrayed BM3h samples (60–100 μl) into microtiter plates and placed them in a 40-cm-bore Bruker Avance 4.7 T MRI scanner, equipped with a 10-cm-inner-diameter birdcage resonator radiofrequency coil and 26 G cm^{-1} triple-axis gradients. We filled unused wells of the microtiter plates with PBS and performed imaging at ~21 °C on a 2-mm slice through the sample. We used a T_1-weighted spin echo pulse sequence; echo time (TE) was 10 ms, and repetition times (TR) were 73, 116, 186, 298, 477, 763 ms, 1.221, 1.953, 3.125 and 5.000 s. Data matrices consisted of 512 × 128 points, zero-filled to 1,024 × 512 points, where the second dimension corresponds to the phase-encoding direction; the field of view (FOV) was 16 × 8 cm. We reconstructed and analyzed images using custom routines running in Matlab and adjusted contrast to optimize MRI images presented in the figures. We calculated relaxation rates by exponential fitting to the image data, using an equation of the form $I = k[1 - \exp(-TR/T1)]$, where I was the observed MRI signal intensity and k was a constant of proportionality. We then determined values of r_1 by linear fitting to a plot of R_1 against protein concentration for six to eight BM3h concentrations in the range from 0 to 240 μM. We also performed low-field relaxivity measurements using benchtop spectrometers operating at 21 °C with proton resonance frequencies of 20 MHz and 60 MHz (Bruker Minispec NMS120 and mq60). Samples of 150 μL containing 50–100 μM BM3h-8C8 in PBS in the absence or presence of 500 μM dopamine yielded 20-MHz relaxivity measurements of 1.0 or 0.25 mM^{-1} s^{-1}, respectively, and 60-MHz relaxivities of 1.1 or 0.23 mM^{-1} s^{-1}, respectively.

Dopamine release from PC12 cells. We grew PC12 cells in suspension in F-12K medium supplemented with 15% (vol/vol) horse serum and 2.5% (vol/vol) FBS (ATCC). In preparation for dopamine release experiments, we incubated 50-ml cell cultures for 1 h in medium supplemented with 1 mM dopamine and 1 mM ascorbic acid, pelleted the cells and washed them twice with Locke's buffer (154 mM NaCl, 5.6 mM KCl, 3.6 mM $NaHCO_3$, 2.3 mM $CaCl_2$, 5.6 mM D-glucose and 5 mM HEPES pH 7.4). To Locke's buffer missing 54 mM NaCl and containing or not containing the sensor, we added a 1:50 dilution of 2.7 M KCl (stimulus) or NaCl (control). We resuspended the washed PC12 cell pellets in 200 μl of either K^+- or Na^+-supplemented buffer, with or without sensor. After 30–60 min incubation at ~21 °C, we pelleted cells and imaged the supernatant in an MRI scanner as described above. We estimated dopamine release by calculating sensor saturation level from observed r_1, then solving the quadratic equation describing bimolecular equilibrium binding with a known K_d, and assuming 32 μM of sensor for ligand concentration. We made independent measurements of dopamine release using the Dopamine EIA Kit (LDN).

Brain injection of sensors with exogenous dopamine. For injection experiments testing the effect of exogenous dopamine on BM3h-8C8 and WT BM3h (**Fig. 5a–c**), we anesthetized adult male Lewis rats with 1–2% isoflurane. We stereotaxically inserted plastic guide cannulae (Plastics One) bilaterally into the striatum and secured them in place with dental cement (coordinates with respect to bregma: +0.7 mm anterior, 3 mm lateral, 6 mm below the surface of the skull). We connected tubing filled with silicone oil to an MRI-compatible dual channel syringe pump (Harvard Apparatus), attached it to internal cannulae and back-filled the cannulae with contrast agent solution, 500 μM BM3h-8C8 or WT BM3h, with or without equimolar dopamine (chemicals from Sigma-Aldrich). We ran the pump in infusion mode for a few seconds to ensure that no air entered the system and then lowered the internal cannulae (connected to the pump) into the implanted guide cannulae and fixed them in place with dental cement. After the implantation was complete, we transferred the animal to a plastic positioning device (Ekam Imaging) for imaging and placed it into a 4.7-T Bruker Avance scanner. We acquired fast spin echo (FSE) MRI scans (TE/TR 14/277 ms, 8.9 s per scan, 0.3 × 0.3 × 1.0 mm resolution, 3.8 × 3.8 cm FOV, data matrix 128 × 128) before infusion (seven scans) and continuously during and after bilateral infusion of paired solutions, each injected for 20 min at 0.5 μl min^{-1}. We monitored heart rate continuously during the infusions using a Nonin Medical 8600V pulse oximeter equipped with a nonmagnetic sensor. We digitized raw oximetry readings using a National Instruments USB-6008 interface and converted them to heart rate using a Matlab code. Values were stable at around 350 beats per minute ± 40 (s.d.).

We analyzed MRI data from these experiments using custom routines running in Matlab. We detrended image signal time courses, converted them to percent change with respect to the preinjection baseline and averaged them over striatal ROIs. ROIs were chosen to approximate the maximal volumes reliably filled with the contrast agent, and were defined by a five-voxel in-plane radius (2.7 mm diameter) around the cannula tips over three image slices centered rostrocaudally around the implantation position, excluding voxels with notable signal dropout due to the cannulae themselves. We produced data for group analyses by combining data from ROIs defined separately with respect

to the injection cannulae tips in each individual. We computed maximal MRI signal changes and signal change maps by averaging the image intensity at the end of the injection period (scans 121–140) and subtracting and normalizing it to the pre-injection intensity (scans 1–7).

Protein and dopamine quantification based on *in vivo* imaging data. We estimated absolute concentrations of contrast agent and dopamine under the assumptions that minimal endogenous dopamine was present, that the relaxivity and dopamine affinity of BM3h variants were the same *in vivo* and *in vitro*, and that the MRI acquisition procedure satisfied a strong T_1-weighting requirement, where TR << T_1. Under these assumptions, the fractional MRI signal change $\Delta I/I_0$ is approximately equal to $\Delta R_1/R_{10}$, the fractional change in R_1 (equal to $1/T_1$). R_{10} is the basal value of R_1, measured as 0.55 ± 0.01 s^{-1} from curve fitting to multiple FSE images obtained with different TR values. We estimated the maximal total concentration of BM3h-8C8 by determining the corresponding ΔR_1 averaged over multiple injections of BM3h-8C8 in the absence of dopamine and dividing it by the relaxivity of the unliganded protein. We determined total dopamine concentration from the value of ΔR_1 observed during injection of BM3h-8C8 plus dopamine, the relaxivities of liganded and unliganded BM3h-8C8, the previously determined BM3h-8C8 concentration and the mass action relationships governing binding of the sensor to dopamine. In *in vitro* measurements, BM3h-8C8 had a T_2 relaxivity of 4 mM^{-1} s^{-1}; addition of 1 mM dopamine did not noticeably perturb this value significantly, suggesting that T_2 effects in conjunction with appropriate imaging methods might be able to provide a basis for protein quantification similar to the approach we describe here.

Histological analysis. After MRI contrast agent injection experiments using the paradigm described above, we placed rats under terminal anesthesia with ketamine and xylazine and transcardially perfused them with phosphate buffer containing heparin (Hospira) and then with 4% wt/vol paraformaldehyde (Sigma-Aldrich). We removed brains and obtained coronal cryosections of 10 µm thickness at 100-µm intervals across a range extending ~1 mm anterior and posterior to the injection cannula insertion site. We used standard protocols for hematoxylin and eosin staining. Terminal deoxynucleotidyl transferase–mediated dUTP nick-end labeling (TUNEL) staining was performed using the DeadEnd Colorimetric TUNEL system from Promega with visualization enhanced by the DAB Substrate Kit from Vector Laboratories. Histological procedures were implemented by Wax-it Histology Services.

***In vivo* potassium stimulation experiments.** For *in vivo* K^+ stimulation experiments (**Fig. 5d–g**), we used isoflurane-anesthetized male Lewis rats. We fitted internal cannulae with Y-connectors and positioned them through bilateral guide cannulae at coordinates 0.8 mm anterior to bregma, 2.8 mm lateral to the midline and 7.8 mm below the skull surface. Each two-channel cannula delivered a given BM3h variant (BM3h-8C8 or WT, paired on opposite hemispheres of the brain; sides were randomized). On each two-channel injection cannula, we loaded one arm with protein in standard artificial cerebrospinal fluid (aCSF, containing 150 mM Na^+ and 3 mM K^+) and the other arm with protein in high-K^+ modified aCSF containing no Na^+ and 153 mM K^+. Two infusion pumps (Harvard Apparatus) drove the infusions; one pump controlled the standard aCSF (low-K^+) infusions on both BM3h-8C8 and WT control sides, and the other pump controlled high-K^+ infusions on both sides. We programmed the two pumps and synchronized them with the MRI experiment so as to acquire a preinfusion image baseline for 2 min, followed by continuous scanning over three stimulation cycles consisting of 10 min low K^+ alternating with 5 min high K^+, followed by a further 10 min of low K^+, followed by up to 30 min of post-injection signal acquisition. During these experiments, we continuously recorded heart rate and found it to be 355 beats per minute ± 45 (s.d.); blood oxygen saturation levels were 94.1 ± 5.8%.

We acquired T_1-weighted multislice MRI scan series as for the dopamine injection experiments described above. We imported raw data into Matlab, processed them with spatial smoothing over nearest neighbors (in-plane) and converted them to percent signal change with respect to a fitted third-order polynomial baseline. Scans from the initial protein-only injection period (<15 min) were excluded from the analysis. To statistically analyze data acquired during the three cycles of K^+ stimulation, we used a procedure analogous to classical fMRI methods, by performing a *t*-test on intensity values associated with high and low K^+ conditions. We considered voxels showing lower signal during the 5-minute intervals corresponding to K^+ stimulation to be consistent with the expected effect of K^+-evoked dopamine release on MRI signal in the presence of BM3h-8C8. We estimated that the delay between infusion pump switching and actual changes to K^+ concentration in the brain was roughly 8–9 min. We derived this estimate by recording the time required for spreading of Trypan blue to a radius of 0.75 mm (comparable to ROIs used for most of the analyses presented) from an injection cannula embedded in 0.6% agarose, in a switched injection paradigm equivalent to the K^+ stimulation paradigm applied *in vivo*. We chose a delay of 9 min for analyses presented in the text, but delays ranging from 7 to 12 min produced qualitatively similar statistical results, all with elevated numbers of voxels near the BM3h-8C8 infusion site showing the expected MRI signal decrease upon K^+ stimulation and far fewer (if any) voxels near the WT BM3h control cannula showing significant ($P < 0.01$) effects (**Supplementary Fig. 5**). We performed ROI-wide computations on cylindrical regions of 1.5 or 2.7 mm diameter in-plane extending over three (1 mm thick) image slices, centered about the BM3h-8C8 and WT BM3h infusion cannula tips, excluding from the calculations voxels showing substantial signal dropout due to the cannulae themselves. We performed group analyses by combining data from ROIs defined separately with respect to injection cannulae in each animal, without further anatomical coregistration.

35. Barnes, H.J., Arlotto, M.P. & Waterman, M.R. Expression and enzymatic activity of recombinant cytochrome P450 17 alpha-hydroxylase in *Escherichia coli*. *Proc. Natl. Acad. Sci. USA* **88**, 5597–5601 (1991).
36. Omura, T. & Sato, R. The carbon monoxide-binding pigment of liver microsomes. I. Evidence for its hemoprotein nature. *J. Biol. Chem.* **239**, 2370–2378 (1964).

doi:10.1038/nbt.1609